

Sun-light driven enhanced azo dye decontamination from aqueous solution by CoO–CuFe₂O₄ derived from layered double hydroxide

Ayodeji Olugbenga Ifebajo, Akeem Adeyemi Oladipo*, Mustafa Gazi

Polymeric Materials Research Laboratory, Chemistry Department, Faculty of Arts and Science, Eastern Mediterranean University, TR North Cyprus, Famagusta via Mersin 10, Turkey, Tel. +903926502406; email: akeem.oladipo@emu.edu.tr/akeem.oladipo@gmail.com (A.A. Oladipo), Tel. +90 3926301110; emails: ayoifebajo@gmail.com (A.O. Ifebajo), mustafa.gazi@emu.edu.tr (M. Gazi)

ABSTRACT

Sun-light driven CoO–CuFe₂O₄ photocatalyst was fabricated successfully from a layered double hydroxide via a modified co-precipitation and calcination method at 500°C, for the decontamination of azo dye-laden wastewater. The CoO–CuFe₂O₄ was characterized and the results demonstrated that it is composed of face-centered cubic CoO and cubic spinel CuFe₂O₄, which has a specific surface area and pore volume of 348.5 m² g⁻¹ and 0.715 cm³ g⁻¹, respectively; and pH point zero charges of 5.8. The photocatalytic activity is enhanced at acidic pH level and achieved ~99.4% decolorization of Eriochrome black T dye (EBT) within 90 min in the presence of 0.05 g of CoO–CuFe₂O₄. Notably, •OH and •O₂⁻ radicals played a role while h⁺ significantly participated during the EBT photodegradation. Reusability experiments confirm that the CoO–CuFe₂O₄ possesses high stability and exhibits efficient photocatalytic reusability with almost the same efficiency for degrading EBT dye.

Keywords: Sun-light driven photocatalysis; Mixed metal oxides; LDH; Azo dye; CoO–CuFe₂O₄

1. Introduction

Azo dyes represent ~68% of dyestuff production globally and are the most widely synthetic colorant released into the environment from textile, leather, printing, cosmetic and paper industries [1–3]. Azo dyes contain one or more azo linkages (–N=N–) in their structure, generally persistent, stable to light, refractory to both anaerobic and aerobic digestions and bio-resistant in the water bodies [2].

The presence of even trace concentration of dyes in the water not only distorts the transparency and aesthetic aspects of the water, but it also presents hazardous effects. Eriochrome Black T (EBT), a mono-azo anionic dye, can be metabolized into diphenylamines such as benzidine (well-known human carcinogen); and nitronaphthalene which causes both hepatic and pulmonary toxicity [4,5]. Therefore, the decontamination of azo dye-laden industrial effluents before they are discharged is of prime importance. Among the commonly reported methods, the photocatalytic process is an efficient and promising technique for the elimination

of organic pollutants even at low concentrations without the formation of secondary hazardous products [1,6,7].

The efficiency of photocatalysts is dependent on the high surface area, suitable morphology, desired band gap, efficient stability and reusability [6–9]. In recent years, researchers have directed their attention towards metal oxide photocatalysts due to their high activity, unique physicochemical as well as optical properties [2,6]. Among these metal oxides, TiO₂ and ZnO have proved their efficiency in degrading a variety of organic pollutants into harmless water and CO₂ [10–12], although their applications are restricted to UV-ray illumination (~3–3.4 eV bandgap) which is 3%–5% of solar flux incident on earth's surface. Unlike single metal oxides (TiO₂), Oladipo et al. [2,6] demonstrated that mixed metal oxide photocatalysts such as CoO–NiFe₂O₄ exhibited narrow bandgap that extends towards visible light region (~42%–45% of solar flux).

Therefore, in this study, CoO–CuFe₂O₄ photocatalyst was fabricated from Co–Fe layered double hydroxide (LDH) intercalated with nitrate ions for decontamination of EBT

* Corresponding author.

containing water. The influence of reaction time, CoO–CuFe₂O₄ dosage, initial dye solution concentration and pH on the EBT discoloration efficiency was investigated. The characteristics results confirmed that CoO–CuFe₂O₄ possesses sufficient specific surface area and suitable magnetic properties. Noticeably, CoO–CuFe₂O₄ exhibited excellent adsorptive and oxidative potentials in an acidic medium within 90 min of sunlight irradiation.

2. Materials and methods

2.1. Materials and reagents

Analytical grade reagents (>99.8%) and distilled water were used in all experiments. Fe(NO₃)₃·9H₂O (Iron(III) nitrate nonahydrate), Cu(NO₃)₂·3H₂O (Copper(II) nitrate trihydrate) were purchased from Carlo Erba Reagents (Spain). Sodium hydroxide, Co(NO₃)₂·6H₂O (cobalt(II) nitrate hexahydrate) and EBT an azo dye (Chemical formula: C₂₀H₁₂N₃O₇SNa, molar mass: 461.4 g mol⁻¹, CI: 14645, λ = 530 nm; acidity (pK_a): 6.2–11.6) were supplied by Sigma-Aldrich (Germany).

2.2. Preparation of CoO–CuFe₂O₄ photocatalyst

Firstly, Co–Fe nitrate LDH was synthesized following our earlier report [2]. Then, 5 g of the Co–Fe nitrate LDH was mixed with a freshly prepared aqueous solution of ~0.065 M Cu(NO₃)₂·3H₂O in a reaction flask and vigorously stirred for 3 h at ambient temperature. The obtained Co/Cu–Fe LDH was filtered, washed severally with 50% ethanol–distilled water solution and dried for 24 h at 60°C. The resulting products were calcined at 500°C (heating rate of 10°C min⁻¹) for 3 h in a muffle furnace, then cooled to room temperature. Finally, the product was ground into a powder and sieved to obtain uniform size (~0.26 mm) CoO–CuFe₂O₄ photocatalyst.

2.3. Characterization

Fourier transforms infrared (FTIR) spectra of the photocatalysts were obtained using an FTIR-8700 spectrophotometer (Perkin-Elmer, Japan). The photocatalyst surface morphology and chemical composition were examined by a scanning electron microscope (JSM-6390, JEOL, Japan) equipped with energy-dispersive X-ray spectroscopy (EDS). The photocatalyst was subjected to nitrogen sorption-desorption isotherms on an Autosorb analyzer (QuantaChrome, USA) at -196°C; and the specific surface area and pore distribution were calculated from the Brunauer–Emmett–Teller and the Barrett–Joyner–Halenda equations, respectively. The crystallinity was obtained by an X-ray diffractometer (Bruker D8, Massachusetts, United States) with a Cu Kα (λ = 1.54187 Å) monochromatic radiation operated at 50 kV, and the crystalline phase was identified using the standard JCPDS file. The ultraviolet-visible reflectance analysis was acquired using a UV-2450 spectrophotometer by Shimadzu (Japan).

2.4. Adsorptive and photocatalytic activity of CoO–CuFe₂O₄

500 mg L⁻¹ EBT stock solution was prepared. The stock solution was serially diluted and linear calibration curves were obtained with R² ≥ 0.993. Firstly, batch experiments were conducted in the dark to acquire the optimum conditions

for EBT decontamination in the presence of CoO–CuFe₂O₄ [2]. The influence of photocatalyst dosage, solution pH and initial concentration of EBT was investigated. The photocatalytic experiments were carried out under direct sunlight from 10:00–15:00 h and the average solar light intensity was recorded by an Apogee Pyranometers (MP-100, USA) as described in our previous paper [11].

Briefly, 0.2–1.3 g L⁻¹ of CoO–CuFe₂O₄ was added to 50 mL of EBT aqueous solution (10–100 mg L⁻¹) in the presence or absence of scavengers (*t*-butyl alcohol (*t*-BuOH), benzoquinone (BQ) and sodium oxalate (Na–O)). The resulting suspension was stirred in the dark for 20 min to reach adsorption–desorption equilibrium and then exposed to sunlight with constant stirring for 6 h. Periodically, 2 mL aliquot sample was withdrawn and the concentration of EBT was measured by a double-beam UV–vis spectrophotometer (T80+ PG Instruments Ltd., UK) at its maximum absorbance wavelength. The solution pH was adjusted (2–12) using 0.1 M HCl and 0.1 M NaOH, and the EBT discolorization efficiency was calculated using the following equation:

$$\text{Discolourization efficiency (\%)} = \left(1 - \frac{C_t}{C_0}\right) \times 100 \quad (1)$$

Here, the initial EBT concentration and concentration after *t* min of reaction/irradiation are represented as C₀ (mg L⁻¹) and C_{*t*} (mg L⁻¹). The measurements were repeated twice and average results are reported within experiment errors (±2%). The spent photocatalyst was desorbed by 0.01 M NaOH, regenerated at 80°C and subjected to successive use–regenerated–reuse cycles.

3. Results and discussion

3.1. Characteristics of the samples

Fig. 1a shows the FTIR spectra of CoO–CuFe₂O₄ before and after the photocatalytic process. The peaks between 3,600 and 3,400 cm⁻¹ are assigned to –OH bond due to the stretching vibrations of the adsorbed interlayered water molecules (δ–HOH) [2,6,13]. The bands at 700–400 cm⁻¹ represent the bending and stretching modes of the metal–oxygen–metal (M–O–M), O–M–O and metal–oxygen (M–O) bonds [13,14]. In particular, absorption peaks at 495, 543, and 655 cm⁻¹ indicates the presence of Cu–O, Fe–O and Co–O [15]. After photocatalytic processes, a slight reduction in intensities of hydroxyl groups and M–O peaks were noticed, however, no significant changes observed.

The nitrogen adsorption–desorption isotherm and pore size distribution for CoO–CuFe₂O₄ is presented in Fig. 1b; with large N₂ uptake at *p/p*₀ ≥ 0.8, it exhibited type IV isotherm with H3 hysteresis associated with slit-like mesopores which are typical of LDH-based materials [23]. The CoO–CuFe₂O₄ specific surface area and pore volumes are 348.5 m² g⁻¹ and 0.715 cm³ g⁻¹ respectively. As shown in Fig. 1b (inset), CoO–CuFe₂O₄ exhibits a broad pore size distribution in the range of 2–8 nm centered at ~5.8 nm with a pore surface area of 14.88 m² g⁻¹. The high specific surface area and wide size distribution range of the mesopores of the CoO–CuFe₂O₄ improved its adsorption capacity for the EBT molecule, resulting in increased photocatalytic activity.

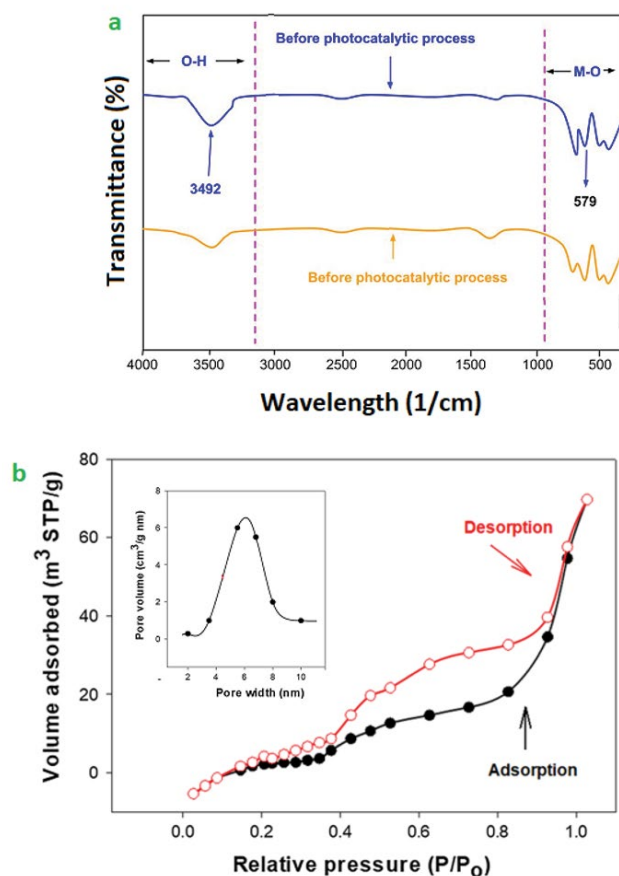


Fig. 1. (a) FTIR spectra and (b) N₂ adsorption/desorption isotherm and pore size distribution (inset) for CoO–CuFe₂O₄.

Fig. 2 shows the X-ray diffraction (XRD) patterns which demonstrated the excellent crystallinity of CoO–CuFe₂O₄. The XRD results showed that CoO–CuFe₂O₄ is composed of cubic spinel CuFe₂O₄ with reflections that match with (111), (202), (311), (400), (511) and (440) planes (JCPDS card no. 034-0425) [16], and face-centered cubic CoO with diffraction peaks at 36.8°, 42.5° and 63.2° corresponding to (111), (200) and (220) lattice planes (JCPDS no. 65-2902) [2]. Note that the intensities of the XRD peaks were slightly weakened after the photocatalytic process. The mean crystallite size of the as-prepared CoO–CuFe₂O₄ nanostructures was calculated by the Scherrer formula ($C_s = 0.9\lambda/\beta \cos\theta$) [11] as 11.5 nm. The θ is the Bragg diffraction angle, λ is the X-ray wavelength and β is the full width at a half-maximum intensity of the 311 reflections.

The surface morphology of CoO–CuFe₂O₄ (Fig. 3a) shows rough and agglomerated hexagonal plate-like particles, which is typical of LDH-based material [2,6]. Also, the EDS spectrum revealed the presence of cobalt, oxygen, copper and iron ions within the CoO–CuFe₂O₄ walls (Fig. 3b). According to the vibrating sample magnetometer analysis, the CoO–CuFe₂O₄ exhibited a magnetic behavior with saturation magnetization ($M_s = 56.8 \text{ emu g}^{-1}$), remanence ($M_r = 3.6 \text{ emu g}^{-1}$) and coercivity (H_c) of 5.5 Oe, suggesting that the CoO–CuFe₂O₄ can be easily separated from sample solution using an external magnetic field. Notably,

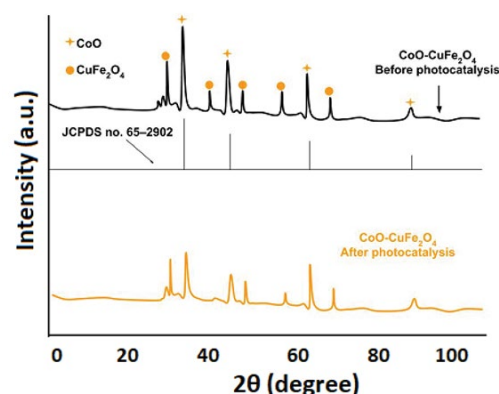


Fig. 2. XRD patterns of CoO–CuFe₂O₄ before and after photocatalysis.

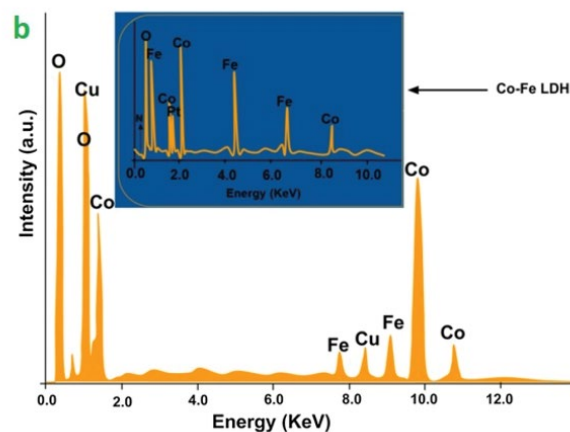
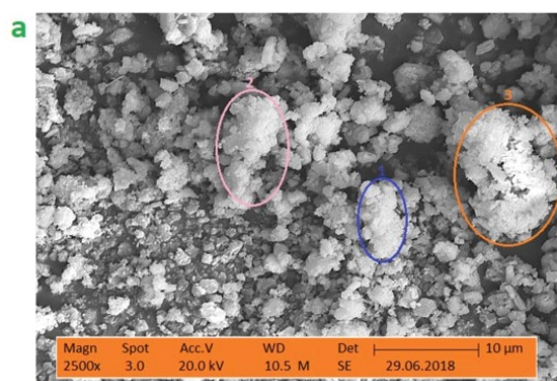


Fig. 3. (a) Scanning electron microscope image and (b) energy-dispersive X-ray of CoO–CuFe₂O₄ [2].

the CoO–CuFe₂O₄ exhibited superparamagnetic behavior due to insignificant coercivity and remanence values [16].

The X-ray photoelectron spectroscopy (XPS) measurement shows the presence of Co, Cu, Fe and O in CoO–CuFe₂O₄. As illustrated in Fig. 4a, the full XPS survey scan spectrum of CoO–CuFe₂O₄ shows Co 2p, O 1s, Cu 2p and Fe 2p peaks at 800, 531, 934 and 710 eV, respectively, which is consistent with earlier reports [16–18]. The spectrum of

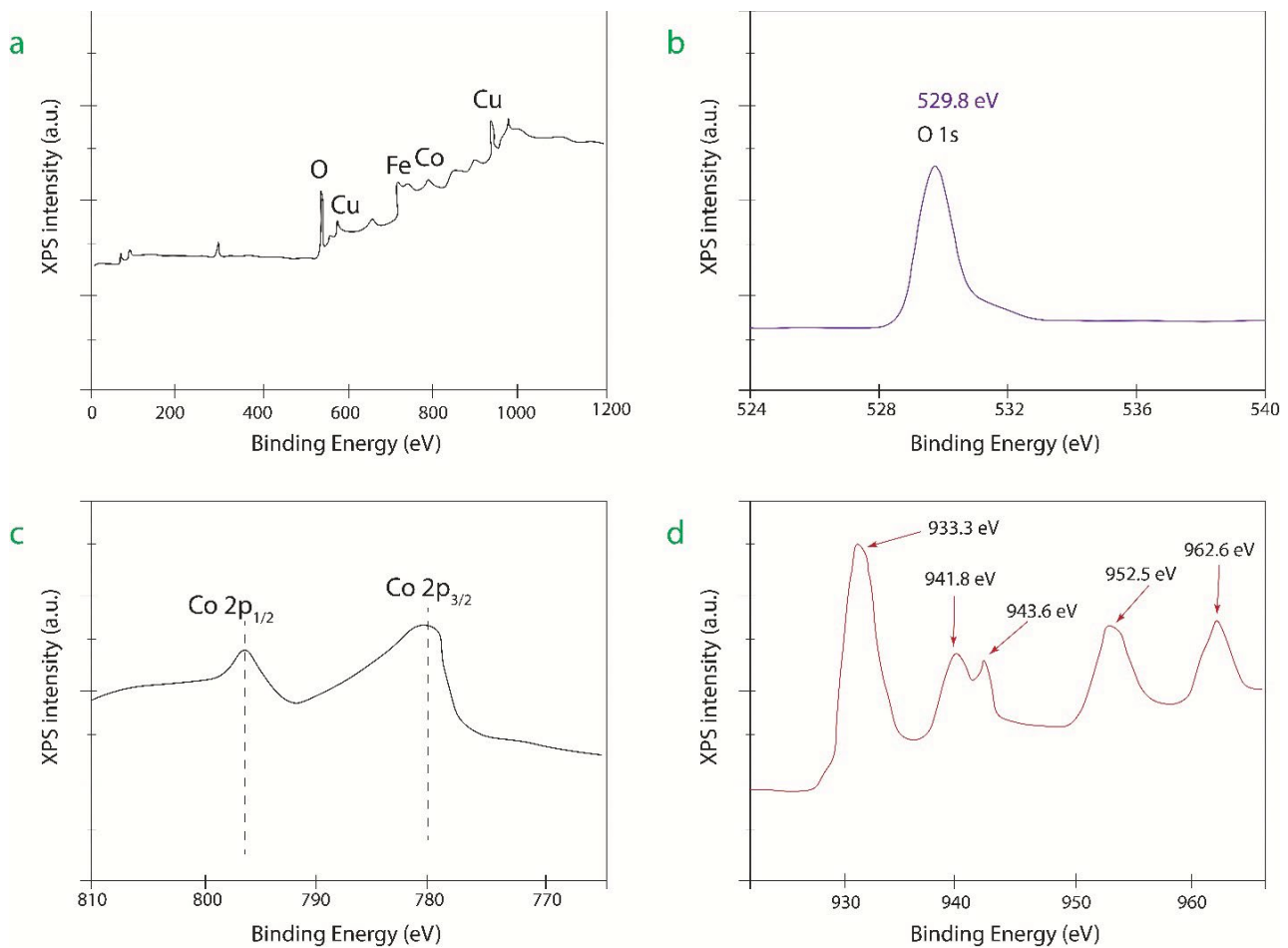


Fig. 4. XPS spectra of the as-prepared CoO–CuFe₂O₄ (a) XPS survey scan, (b) O 1s, (c) Co 2p, and (d) Cu 2p.

O 1s (Fig. 4b) with binding energy at 529.8 eV is ascribed to lattice oxygen [17]. Fig. 4c shows the Co 2p spectrum characterized by two peaks at a binding energy of 781 and 797 eV for Co 2p_{3/2} and Co 2p_{1/2}, respectively. The spectrum of Cu 2p is presented in Fig. 4d with five peaks. The peaks located at 933.3 and 952.5 eV correspond to Cu 2p_{3/2} and Cu 2p_{1/2}, respectively. The satellite peaks at 941.8 and 962.6 eV confirmed the presence of copper oxide species in CoO–CuFe₂O₄.

3.2. Effect of operational parameters

To assess the performance of CoO–CuFe₂O₄ and achieve efficient photocatalytic decontamination of EBT, the influence of key operational parameters was evaluated. The time-dependent discolorization of EBT in the dark shows that 60% of the color was removed within 60 min and progressed smoothly until 180 min where 95.5% color was removed as illustrated in Fig. 5a. No significant degradation of EBT was observed in sunlight in the absence of the CoO–CuFe₂O₄ (photolysis); after 180 min of reaction, ~10.5% discolorization was achieved. In contrast, 83% discolorization was achieved in the first 60 min in the presence of sunlight/CoO–CuFe₂O₄ and rapidly increased to nearly 100% after 90 min. The results suggested that the EBT discolorization

is majorly driven by the synergistic effect of adsorption and photocatalytic degradation.

3.3. Effects of initial pH on the performance of CoO–CuFe₂O₄

The effect of pH in the range of 2–10 on the photocatalytic degradation of EBT was investigated under sunlight irradiation in the presence of 0.05 g CoO–CuFe₂O₄ with an initial dye concentration of 20 mg L⁻¹. The pH_{pzc} (pH point zero charge) of CoO–CuFe₂O₄ was determined via the pH drift method as 5.8 [2], suggesting that the surface is positively charged in acidic solutions (at pH < 5.8) and negatively charged at pH > 5.8. Fig. 5b shows that higher degradation was observed in an acid medium (pH < 5); notably, CoO–CuFe₂O₄ exhibited the highest EBT discolorization, reaching ~99.4% at pH 2.0 and then decreased to 80.7% and 55.8% as the pH is further increased to pH 3.0 and 4.0, respectively. At lower pH, the negatively charged EBT molecules (pK_a values at 6.6 and 11.6, having one sulfonated (–SO₃⁻) group) were adsorbed electrostatically by the positively charged active sites of CoO–CuFe₂O₄, where the photogenerated hydroxyl radicals (•OH) attacked the aromatic rings resulting in azo bond cleavage (chromophoric group destruction) [6,19].

In the alkaline solution (pH 10), 3.5% discolorization was achieved after 120 min sunlight irradiation; this might

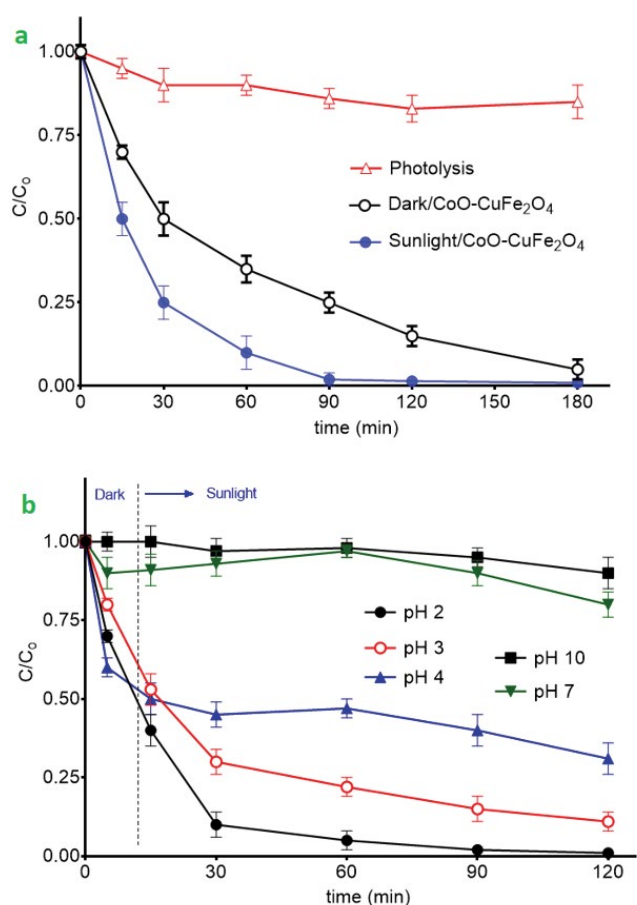


Fig. 5. (a) Comparative performance of different processes for decolorization of EBT and (b) variation of solution pH on the performance of CoO-CuFe₂O₄ (Reaction conditions: 0.05 g CoO-CuFe₂O₄, 20 mg L⁻¹ EBT and 180 min reaction time).

be due to the repulsion of EBT-SO₃⁻ ions by the negatively charged CoO-CuFe₂O₄ (pH > p*H*_{pzc}). Also, the OH⁻ anions in the alkaline solution and the negatively charged surface of CoO-CuFe₂O₄ would limit the formation of •OH radicals leading to a reduced photodegradation efficiency [19]. Similarly, Ma et al. [20] and Konyar et al. [21] reported that an acidic environment enhances •OH production and minimizes electron-holes recombination which is beneficial for photocatalytic degradation of azo dyes. Their results are consistent with the results reported herein.

3.4. Effects of CoO-CuFe₂O₄ dosage and initial concentration of EBT

A series of experiments were performed by varying the dose of CoO-CuFe₂O₄ from 0.01 to 0.065 g L⁻¹ to investigate the influence of the photocatalyst amounts. Fig. 6a shows that the discolorization efficiency increased significantly from 40% to 99.3% when the dosage of CoO-CuFe₂O₄ increases from 0.01 to 0.05 g L⁻¹ during the first 90 min. This is obviously attributed to the increase of the CoO-CuFe₂O₄ active sites, resulting in enhanced •OH radical formation [6,22].

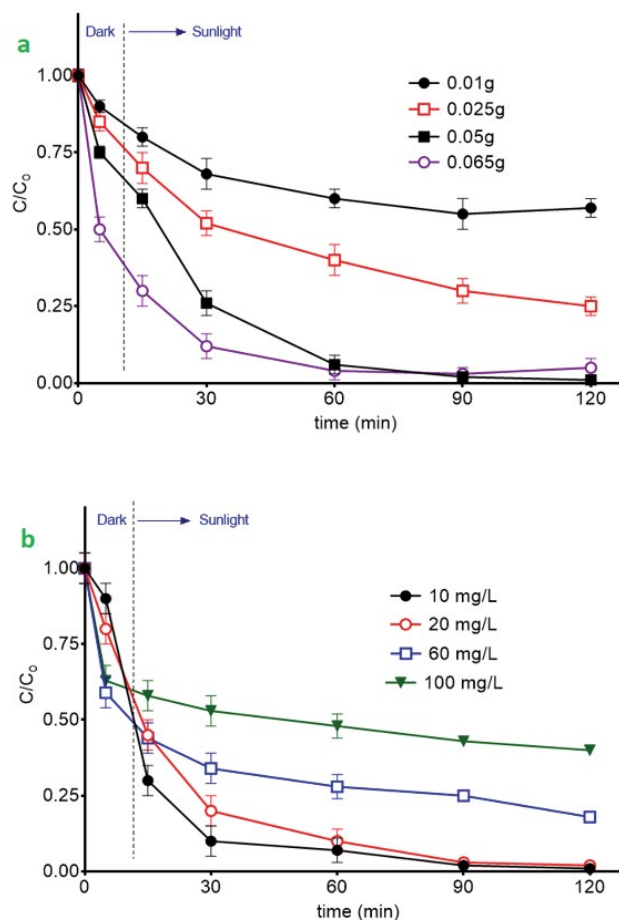


Fig. 6. Effects of (a) photocatalyst dosage and (b) initial EBT concentration on decolorization efficiency of CoO-CuFe₂O₄ (Reaction conditions: pH 2.0 and 120 min reaction time).

However, increasing the CoO-CuFe₂O₄ dosage beyond 0.05 to 0.065 g L⁻¹ led to a slight reduction in the discolorization efficiency which is notable at 120 min, due to an increase in the turbidity of the suspension and subsequent decrease in sunlight penetration [6,22–24]. Note that, the discolorization efficiency was rapid at the initial stage (first 60 min) followed by a slower rate from 60 to 120 min. The slow discolorization rate beyond 60 min is possibly due to the saturation of the sorption sites of the CoO-CuFe₂O₄ [6].

Fig. 6b indicates that discolorization efficiency decreases with the increase in the initial concentration of EBT. At 90 min, the discolorization rate decreased from 99.4% to 73% and 52.6% when the EBT initial concentration increased from 10 to 60 and 100 mg L⁻¹, respectively. This is because more and more EBT molecules were adsorbed on the CoO-CuFe₂O₄ surface when the initial concentration increases, thus, reducing the generation of hydroxyl radicals and consequently the photodegradation efficiency is reduced.

3.5. Mineralization and identification of reactive oxidative species

The mineralization of the EBT solution was monitored at pH 2.0 and 4.0, and the results are presented in Fig. 7a.

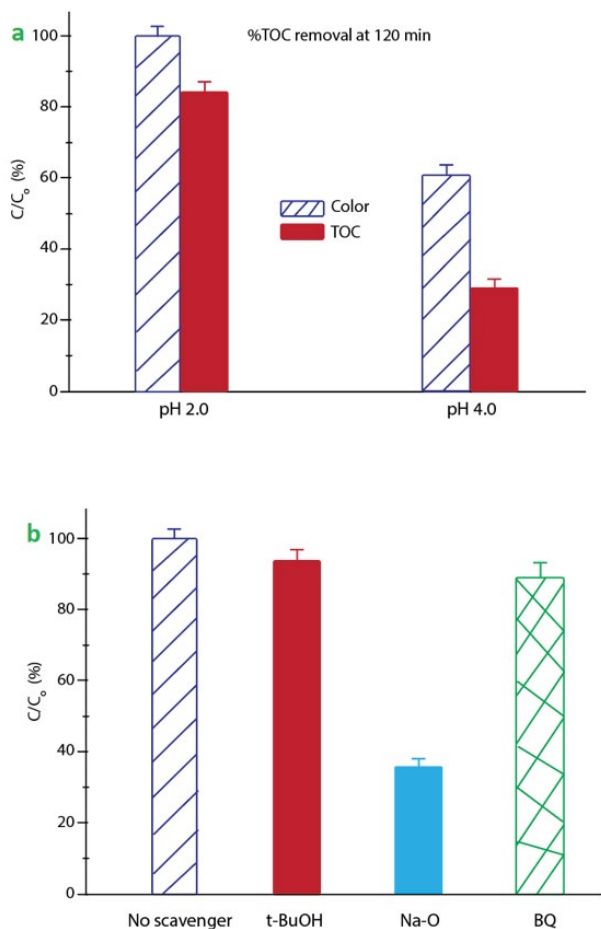


Fig. 7. (a) Comparison of EBT mineralization and discolorization by CoO–CuFe₂O₄ and (b) effect of scavenger supplementation on the photocatalytic degradation of EBT (Reaction conditions: pH 2.0, 20 mg L⁻¹ EBT, 0.05 g CoO–CuFe₂O₄ and 120 min reaction time).

The results showed that at pH 2.0, the EBT was completely decolorized, while 84% of total organic carbon (TOC) was removed after 120 min of irradiation, suggesting that complete mineralization was not achieved and some intermediate organic species remained in solution. As expected, at pH 4.0, 60% discolorization was achieved while the TOC decreased from 38.9 mg L⁻¹ at '0 min' to 9.5 mg L⁻¹ after 120 min, achieving ~28.8% mineralization only.

To investigate the reactive oxidative species that participated in the EBT photodegradation process, various radical scavengers were tested. 5 mM of tert-butyl alcohol (*t*-BuOH), BQ and sodium oxalate (Na–O) were added as scavengers to trap $\cdot\text{OH}$, $\cdot\text{O}_2^-$ and h^+ , respectively [11,17]. Fig. 7b shows that the addition of *t*-BuOH and BQ decreased the photocatalytic degradation of EBT slightly by 5.5% and 10% respectively, implying that $\cdot\text{OH}$ and $\cdot\text{O}_2^-$ were not the dominant active species during the EBT photocatalytic process. However, after the addition of Na–O, the photodegradation of EBT decreased by 65.4% in 90 min, demonstrated that the photocatalytic process was majorly governed by photogenerated holes (h^+).

3.6. CoO–CuFe₂O₄ stability and recyclability

The stability and reusability of the CoO–CuFe₂O₄ photocatalyst was conducted via six successive use–regenerate–reuse cycles with 0.05 g spent catalyst and 10 mg L⁻¹ initial EBT concentration. Each cycle was performed initially in the dark for 20 min and then exposed to sunlight for 120 min. No significant changes were noticed in the structural integrity of CoO–CuFe₂O₄ after six cycles of use as determined by FTIR and XRD suggesting that the CoO–CuFe₂O₄ is highly stable. Meanwhile, the photocatalytic efficiency reduced from 95.8% during the first cycle to 77.8% during the sixth cycle (Fig. 8). Also, the TOC removal efficiency decreases from ~78% to 42.6% in 6 cycles. The CoO–CuFe₂O₄ was submerged in distilled water for 3 d and the concentration of leached cobalt, iron and copper ion in the solution was in the range of 0.05–0.28 mg L⁻¹ leached metal ion concentration was analyzed to evaluate the stability of the catalyst. Suggesting that the CoO–CuFe₂O₄ is a potential catalyst with excellent recyclability, high stability, and photocatalytic activity.

3.7. Photocatalytic degradation mechanism of CoO–CuFe₂O₄

Considering the ultraviolet–vis diffuse reflectance spectra and photoluminescence spectrum, the bandgap energy of CoO–CuFe₂O₄ was determined as 2.1 eV as well as its VB (valence band = 1.42 eV) and CB (conduction band = –0.68 eV) according to the equations reported in our recent reports [6,22]. Here, CoO–CuFe₂O₄ is activated with sunlight and photoexcited electrons migrated from the VB to the CB with the formation of photogenerated electron–hole pairs (e^-/h^+), which is able to reduce and/or oxidize the adsorbed EBT on the CoO–CuFe₂O₄ surface.

Since the reduction potential of $\text{O}_2/\cdot\text{O}_2^-$ (–0.33 eV vs. NHE) is less negative than the CB of the CoO–CuFe₂O₄ (–0.68 eV), the photogenerated e^- at the CB directly reduced O_2 into $\cdot\text{O}_2^-$ which directly degraded the adsorbed EBT into harmless intermediates. Note that, the VB potential of CoO–CuFe₂O₄ (1.42 eV) is more positive than that of $\text{O}_2/\text{H}_2\text{O}$ (1.23 eV) and can easily induce the formation of $\cdot\text{OH}$

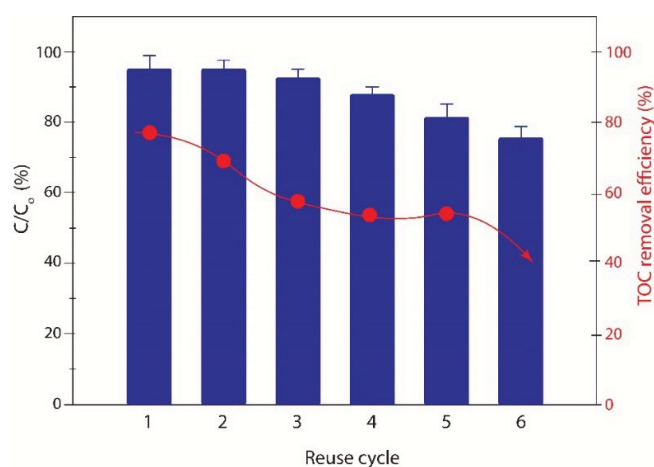


Fig. 8. Recyclability and stability experiments for CoO–CuFe₂O₄ (Reaction conditions: pH 2.0, 20 mg L⁻¹ EBT, 0.05 g CoO–CuFe₂O₄ and 120 min reaction time).

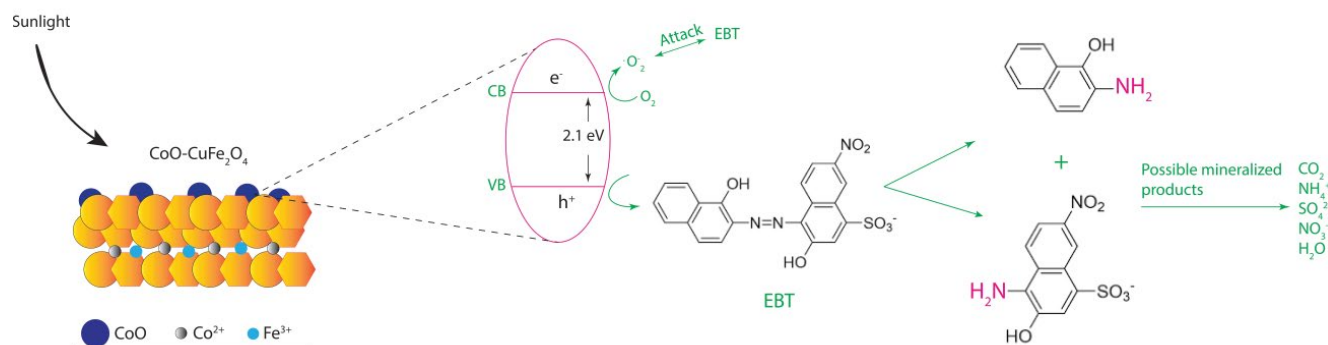


Fig. 9. Schematic illustration of the photocatalytic degradation of EBT by CoO–CuFe₂O₄.

Table 1
Comparison of degradation percentage of EBT dye using CoO–CuFe₂O₄ with literature

Catalyst	Synthesis method	Dosage (g)	Light source	Degradation efficiency (%)	Time (min)	Ref.
CoO–CuFe ₂ O ₄	Co-precipitation	0.05	Sunlight	~99.4	90	This study
Ho ₂ O ₃	Hydrothermal	0.04	UV light	80	100	[25]
NiO _{11.2%} –ZnO _{6.0%} –NZX	Hydrothermal	0.10	UV light	80	90	[26]
CoO–NiFe ₂ O ₄	Co-precipitation	0.05	Sunlight	95.4	120	[6]
Nd ₂ Zr ₂ O ₇	Solvothermal	0.12	UV light	84	50	[27]
ZnO	Thermal decomposition	1.00	UV light	80	90	[28]
ZnO	Commercial	0.30	UV-A light	83	20	[29]
NiS–P zeolite	Solvothermal, ion-exchange	0.80	UV light	~67.5	180	[1]
SWCNT/Nd,N,Se–TiO ₂	Solvothermal, precipitation	0.10	Simulated solar light	89.2	240	[30]

from OH groups of the CuFe₂O₄–LDH based hierarchical structure. Besides the significant contribution of the h⁺, the [•]O₂⁻ and hydroxyl radicals played a role in the photocatalytic oxidation process, which is consistent with the scavenger trapping experiments.

The increased photoactivity of the CoO–CuFe₂O₄ is attributed to the efficient separation of the photoexcited electron–hole pairs due to the high dispersion of CoO on the CuFe₂O₄–LDH based hierarchical structure [13–17]. Considering the observed results herein and our recent report [6], the probable degradation pathway for EBT is shown in Fig. 9, where EBT molecules are decomposed by the h⁺ or [•]O₂⁻ releasing the benzene-containing intermediates such as 5-Amino-1-naphthol and benzene sulfonate, and subsequent possible mineralized products (CO₂, SO₄²⁻, NO₃⁻, H₂O and NH₄⁺).

3.8. Comparison of photocatalytic degradation efficiency of CoO–CuFe₂O₄ towards EBT dye with available literature

Table 1 shows the comparison between the experimental conditions in the present research and studies conducted by researchers regarding the photocatalytic degradation of EBT. It is worthy to mention that, the photocatalytic decolorization of EBT by CoO–CuFe₂O₄ was more favorable than those of other photocatalysts considering the dosage, treatment

time and the fact that CoO–CuFe₂O₄ potential was harnessed directly under sunlight.

4. Conclusion

In this research, we demonstrated a simple and facile synthesis of CoO–CuFe₂O₄ from Co–Fe LDH which is confirmed to be an excellent sunlight-light driven photocatalyst for decontamination of dye-containing wastewater. The photocatalytic activity of CoO–CuFe₂O₄ increased at an acidic medium, specifically at pH < 4 reaching ~99% discolorization of EBT (an azo dye) within 90 min of sunlight irradiation. Notably, the CoO–CuFe₂O₄ is highly stable with a consistently high degree of EBT degradation for six consecutive catalytic reuse cycles. Both the [•]O₂⁻ and OH[•] radicals are proved to play a role in the photocatalytic process, while h⁺ was the dominant reactive species according to scavenger quenching experiments. Noticeably, the structural integrity and characteristic surface functional groups of the recovered spent CoO–CuFe₂O₄ photocatalyst was almost the same after consecutive use, suggesting that CoO–CuFe₂O₄ has a great potential in wastewater treatment.

Acknowledgment

The authors would like to thank the entire committee of the 2nd International Conference on Water Problems in

the Mediterranean Countries (WPMC 2019), North Cyprus for providing careful and useful suggestions during the conference.

References

- [1] A.N. Ejhieh, M. Khorsandi, Photodecolorization of Eriochrome Black T using NiS-P zeolite as a heterogeneous catalyst, *J. Hazard. Mater.*, 176 (2010) 629–637.
- [2] A.O. Ifebajo, A.A. Oladipo, M. Gazi, Efficient removal of tetracycline by CoO/CuFe₂O₄ derived from layered double hydroxides, *Environ. Chem. Lett.*, 17 (2019) 487–494.
- [3] A.A. Oladipo, M. Gazi, E. Yilmaz, Single and binary adsorption of azo and anthraquinone dyes by chitosan-based hydrogel: selectivity factor and Box-Behnken process design, *Chem. Eng. Res. Des.*, 104 (2015) 264–279.
- [4] H.B. Hadjiltaiefa, S.B. Ameer, P.D. Costa, M.B. Zina, M.E. Galvez, Photocatalytic decolorization of cationic and anionic dyes over ZnO nanoparticle immobilized on natural Tunisian clay, *Appl. Clay Sci.*, 152 (2018) 148–157.
- [5] F.M.D. Chequer, D.J. Dorta, D.P. de Oliveira, Azo Dyes and their Metabolites: Does the Discharge of the Azo Dye Into Water Bodies Represent Human and Ecological Risks?, P. Hauser, Ed., *Advances in Treating Textile Effluent*, InTech, London, United Kingdom, 2011.
- [6] A.A. Oladipo, A.O. Ifebajo, M. Gazi, Magnetic LDH-based CoO–NiFe₂O₄ catalyst with enhanced performance and recyclability for efficient decolorization of azo dye via Fenton-like reactions, *Appl. Catal., B*, 243 (2019) 243–252.
- [7] S.M. Saleh, ZnO nanospheres based simple hydrothermal route for photocatalytic degradation of azo dye, *Spectrochim. Acta, Part A*, 211 (2019) 141–147.
- [8] A.B. Djuricic, Y.H. Leung, A.M.C. Ng, Strategies for improving the efficiency of semiconductor metal oxide photocatalysis, *Mater. Horiz.*, 1 (2014) 400–410.
- [9] D. Bhattacharya, D. Ghoshal, D. Mondal, B.K. Paul, N. Bose, S. Das, M. Basu, Visible light driven degradation of brilliant green dye using titanium based ternary metal oxide photocatalyst, *Res. Phys.*, 12 (2019) 1850–1858.
- [10] M.M. Khan, S.F. Adil, A. Al-Mayouf, Metal oxides as photocatalysts, *J. Saudi Chem. Soc.*, 19 (2015) 462–464.
- [11] M. Gazi, A.A. Oladipo, Z.E. Ojoro, H.O. Gulcan, High-performance nanocatalyst for adsorptive and photo-assisted Fenton-like degradation of phenol: modeling using artificial neural networks, *Chem. Eng. Commun.*, 204 (2017) 729–738.
- [12] Z. Xing, J. Zhang, J. Cui, J. Yin, T. Zhao, J. Kuang, Z. Xiu, N. Wan, W. Zhou, Recent advances in floating TiO₂-based photocatalysts for environmental application, *Appl. Catal., B*, 225 (2018) 452–467.
- [13] J. Ma, J. Ding, L. Yu, L. Li, Y. Kong, S. Komarneni, BiOCl dispersed on NiFe–LDH leads to enhanced photo-degradation of Rhodamine B dye, *Appl. Clay Sci.*, 109–110 (2015) 76–82.
- [14] D. Sun, D. Chi, Z. Yang, Z. Xing, J. Yin, Z. Li, Q. Zhu, W. Zhou, Mesoporous g-C₃N₄/Zn–Ti LDH laminated van der Waals heterojunction nanosheets as remarkable visible-light-driven photocatalysts, *Int. J. Hydrogen Energy*, 44 (2019) 16348–16358.
- [15] D. Chen, Y. Li, J. Zhang, J. Zhou, Y. Guo, H. Liu, Magnetic Fe₃O₄/ZnCr-layered double hydroxide composite with enhanced adsorption and photocatalytic activity, *Chem. Eng. J.*, 185–186 (2012) 120–126.
- [16] Z. Cao, C. Zuo, H. Wu, One step for synthesis of magnetic CuFe₂O₄ composites as Photo-Fenton catalyst for degradation organics, *Mater. Chem. Phys.*, 237 (2019) 121842.
- [17] Z. Li, C. Guo, J. Lyu, Z. Hu, M. Ge, Tetracycline degradation by persulfate activated with magnetic Cu/CuFe₂O₄ composite: efficiency, stability, mechanism and degradation pathway, *J. Hazard. Mater.*, 373 (2019) 85–96.
- [18] T.B. Nguyen, R. Doong, C.P. Huang, C.W. Chen, C.D. Dong, Activation of persulfate by CoO nanoparticles loaded on 3D mesoporous carbon nitride (CoO@meso-CN) for the degradation of methylene blue (MB), *Sci. Total Environ.*, 675 (2019) 531–541.
- [19] S. Mortazavian, A. Saber, D.E. James, Optimization of photocatalytic degradation of acid blue 113 and acid red 88 textile dyes in a UV-C/TiO₂ suspension system: application of response surface methodology (RSM), *Catalysts*, 9 (2019) 360, <https://doi.org/10.3390/catal9040360>.
- [20] C.M. Ma, G.B. Hong, H.W. Chen, N.T. Hang, Y.S. Shen, Photooxidation contribution study on the decomposition of azo dyes in aqueous solutions by VUV-based AOPs, *Int. J. Photoenergy*, 2011 (2011) 1–8.
- [21] M. Konyar, T. Yildiz, M. Aksoy, H.C. Yatmaz, K. Öztürk, Reticulated ZnO photocatalyst: efficiency enhancement in degradation of Acid Red 88 azo dye by catalyst surface cleaning, *Chem. Eng. Commun.*, 204 (2017) 711–716.
- [22] A.A. Oladipo, MIL-53 (Fe)-based photo-sensitive composite for degradation of organochlorinated herbicide and enhanced reduction of Cr (VI), *Process Saf. Environ. Prot.*, 116 (2018) 413–423.
- [23] Z.M. Zangi, H. Ganjidoust, B. Ayati, Analysis of photocatalytic degradation of azo dyes under sunlight with response surface method, *Desal. Wat. Treat.*, 63 (2017) 262–274.
- [24] D. Chen, W. Wang, F. Zhang, Y. Yang, G. Qian, Visible light photocatalytic degradation of methylene blue by H₂O₂/NiFe₂O₄ synthesized from wastewater, *Desal. Wat. Treat.*, 96 (2017) 169–177.
- [25] S. Mortazavi-Derazkola, S. Zinatloo-Ajabshir, M. Salavati-Niasari, Facile hydrothermal and novel preparation of nanostructured Ho₂O₃ for photodegradation of eriochrome black T dye as water pollutant, *Adv. Powder Technol.*, 28 (2017) 747–754.
- [26] M. Karimi-Shamsabadi, M. Behpour, A.K. Babaheidari, Z. Saberi, Efficiently enhancing photocatalytic activity of NiO–ZnO doped onto nanozeoliteX by synergistic effects of p-n heterojunction, supporting and zeolite nanoparticles in photo-degradation of Eriochrome Black T and Methyl Orange, *J. Photochem. Photobiol., A*, 346 (2017) 133–143.
- [27] S. Zinatloo-Ajabshir, M. Salavati-Niasari, Photo-catalytic degradation of erythrosine and eriochrome black T dyes using Nd₂Zr₂O₇ nanostructures prepared by a modified Pechini approach, *Sep. Purif. Technol.*, 179 (2017) 77–85.
- [28] J. Kaur, S. Singhal, Highly robust light driven ZnO catalyst for the degradation of eriochrome black T at room temperature, *Superlattices Microstruct.*, 83 (2015) 9–21.
- [29] K.M. Lee, S.B. Abdul Hamid, C.W. Lai, Multivariate analysis of photocatalytic-mineralization of Eriochrome Black T dye using ZnO catalyst and UV irradiation, *Mater. Sci. Semicond. Process.*, 39 (2015) 40–48.
- [30] G. Mamba, X.Y. Mbianda, A.K. Mishra, Enhanced visible light photocatalytic degradation of eriochrome black T and eosin blue shade in water using tridoped titania decorated on SWCNTs and MWCNTs: effect of the type of carbon nanotube incorporated, *Mater. Chem. Phys.*, 149–150 (2015) 734–742.